AIAA AVIATION Forum
5-9 June 2017, Denver, Colorado
47th AIAA Fluid Dynamics Conference

10.2514/6.2017-3813

An Experimental Study on Small UAV Propellers with Serrated Trailing Edges

Zhe Ning[1], Richard Wlezien[2], Hui Hu[3](✉)
Department of Aerospace Engineering, Iowa State University, Ames, Iowa, 50011

Saw-tooth serration, a bio-inspired geometry, was applied to the trailing edge to accomplish noise attenuation at large Reynolds numbers ($10^5 \sim 1.6\times10^6$) in previous studies. In the current research, three different serration sizes were added to the baseline propeller to determine the noise attenuation potential of the serration on a small UAV propeller operating at a low Reynolds number (Re=53,000). The experiments were conducted at hover and forward flight conditions. Aerodynamic forces, sound pressure levels, and downstream flow fields were measured in order to compare the aerodynamic and aeroacoustic characteristics between baseline propeller and saw-tooth serrated trailing edge (SSTE) propellers. It was discovered that the propellers with SSTE could reduce the noise level at high frequency. Furthermore, an increase in serration size resulted in a noise attenuation effects increasing has been found. The force measurements revealed that the SSTE propellers could generate equal thrust to the baseline propeller under a constant power input. The flow field measurements illustrated that the SSTE propellers had a limited effect on the mean flow. However, the serration will significantly affect the flow passing the trailing edge by varying the velocity and the wake geometry.

Nomenclature

BPL	=	Blade passing frequency
c	=	Chord length of the propeller
c_{tip}	=	Chord length at the tip of the propeller
c_r	=	Chord length at corresponding radius of the propeller
D	=	Diameter of the propeller
h	=	Half of the serration height
R_{e_c}	=	Reynolds number at corresponding chord length
p	=	Sound pressure
p_{ref}	=	Sound pressure reference
R	=	Radius of the propeller
r	=	Non-dimensional radial distance
SPL	=	Sound pressure level
t	=	Thickness of the trailing edge
x	=	Axial coordinate
y	=	Vertical coordinate
z	=	Transverse coordinate
α	=	Angle of attack
λ	=	Width of the serration
δ^*	=	Boundary layer displacement thickness

I. Introduction

In past several decades, Unmanned Aerial Vehicles (UAVs) have become a hot topic in both industry and academic fields. With the reduction of the size and cost of small electronic devices (e.g., processors, sensors, and batteries), the

[1] Graduate Student, Department of Aerospace Engineering.
[2] Professor and Vance and Arlene Coffman Endowed Department Chair of Aerospace Engineering. AIAA Fellow
[3] Martin C. Jischke Professor of Aerospace Engineering, AIAA Associate Fellow, Email: huhui@iastate.edu

progress in the development of small UAVs has been very rapid[1]. According to the BI intelligence, from 2015 to 2020, the annual growth rate of small commercial UAVs is expected to be 19%, which will result in 22 million small UAV shipments by the year 2020[2]. Furthermore, the global market of small UAVs will reach around 10 Billion USD by 2020[3]. Due to its hovering ability and vertical take-off and landing (VTOL) motion, the rotary-wing system has become a popular platform, and has gained more attentions compared with fixed wing and flapping wing aircraft[4]. With these attributes, rotary-wing UAVs have been used for many civilian applications, such as, video taking, construction, deliveries, rescue operations, and personal entertainment. Commonly, the rotary-wing UAV has an even number of rotors and are designed into two sets which either rotate in the clockwise (CW) or counter-clockwise (CCW) direction in order to balance the aerodynamic torque and angular acceleration about the yaw axis. Different from the fixed wing aircraft, the rotary-wing UAV achieves pitch, roll and yaw motions based on varying the rotational speed of propellers.

With the development of control theory, rotary-wing UAVs could fly stably to accomplish many tasks. However, the aeroacoustic noise generated by such a craft is an essential problem associated with it. The aerodynamics noise generated from an operating rotary-wing UAV could affect human life, as well as wild animals. As shown in figure 1 (a), due to the noise effect of UAVs on nesting peregrine falcons, the park restricts the use of drones. In the research work done by Ditmer et al[5], the noise generated from UAVs could significantly increase the heart rate of bears, which indicated an undesirable stress response. Therefore, reducing the noise from rotary-wing UAVs is necessary. Meanwhile, the reduction of the noise would greatly broaden the range of missions for small UAVs according to Leslie[6] and Sinibaldi[7].

Propellers, the main lift generating component of rotary-wing UAVs, transfer electric power into kinetic energy. Aerodynamic noise is generated due to the rotation of the propellers. The aerodynamic noise generated from rotary wings usually consists of inflow turbulence noise as well as airfoil self-noise. Comparing these two sources, the airfoil self-noise contributes a larger percentage to the total noise. Five types of airfoil self-noise generation mechanisms had been classified by Brooks[8]. Within these five categories, four of them are associated with the flow interaction between turbulent and trailing edge. By modifying the trailing edge with a saw-tooth serration, which is a bio-inspired geometry, noise attenuation could be achieved based on previous theoretical and experimental studies. According to the analytical analysis done by Howe[9,10], and an experimental study done by Gruber[11,12], the serration will decrease the scattering efficiency and result in noise reduction. Moreau[13] and Herr[14] conducted experiments to illustrate that the serrated trailing edge also has the potential to reduce the vortex shedding noise when the trailing edge thickness is large than 0.3 boundary-layer displacement thickness. From an aerodynamics perspective (Gruber[11], 2010, Oerleman[15] , and Moreau[13]), the saw-tooth serrated trailing edge has no significant effect on lift. However, it will increase the drag coefficient, the turbulence, as well as the wake size. This indicates that the serration would increase the turbulent mixing and reduce the correlation length of turbulence at trailing edge. In Oerlemans's research work, it was discovered that broadband noise could be reduced substantially by adding the saw-tooth serration to the trailing edge of a wind turbine prototype[15].

Figure 2 shows the geometry of a typical saw-tooth serration, where 2h is the serration height (or amplitude), λ is the width, and Θ is the inclined angle. According to Howe[10], in order to use the saw-tooth serration at the propeller trailing edge to reduce noise, some important geometry parameters need to be considered. The ratio between half height of the serration and the boundary layer thickness at trailing edge (h/δ) should larger than 0.25, otherwise the amplitude of the serration would be too small, and the turbulent eddies would pass over the saw-tooth without significant interaction. Thus, the system will experience no noise reduction. Secondly, the inclined angle should smaller than 45 degrees, which means the width/height ratio (λ/h) of the serration will smaller than 4.

While the saw-tooth serration has been tested near the trailing edges of flat plates, symmetric and asymmetric airfoils, and wind turbine blades at relatively high Reynolds numbers, very little can be found in literature to examine the effects of serrated trailing edges on the aerodynamic and aeroacoustic performances of small UAV propeller operation at much lower Reynolds numbers ($\sim 10^4$). With this in mind, we conducted the present experimental study to characterize the aerodynamic and aeroacoustic performances of small UAV propellers with serrated trailing edges under hover and forward flight conditions. This was done in order to improve our understanding about the effects of saw-tooth serrated trailing edges on the aerodynamic forces, noise generation, and flow structure characteristics in the wakes of UAV propellers.

(a) (b)

Figure 1. Noise generated by UAVs may affect animals

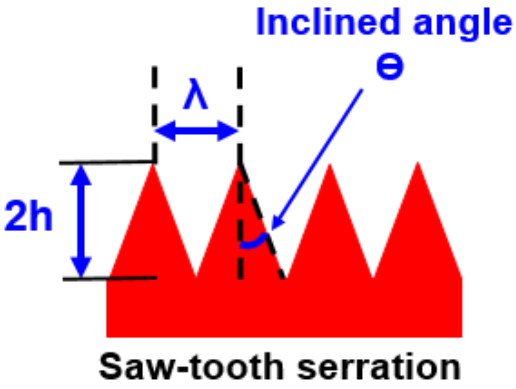

Figure 2. Saw tooth serration geometry

II. Propeller Models Design and Experimental Setup

2.1 Propeller design

Figure 3 shows the schematics of the baseline propeller used in the present study. In order to accomplish 3N designed thrust, an E63 airfoil (low Reynolds number airfoil) was used to design the baseline propeller [16]. The thickness of the airfoil was doubled along the camber line due to a strength concern. The propeller is 240mm in diameter and yields an 8mm tip chord. The chord lengths along the propeller radius from tip to 30% radius were calculated by the optimal chord length equation $C_r = \frac{C_{tip}}{r}$, where C_r is the chord length at corresponding radius location, and r represents a non-dimensional radial distance, which is 0 in the rotating center and 1 at tip. The blade twist angle is 11.6 degrees at the tip, and 28.1 degrees at the 30% radius from the root.

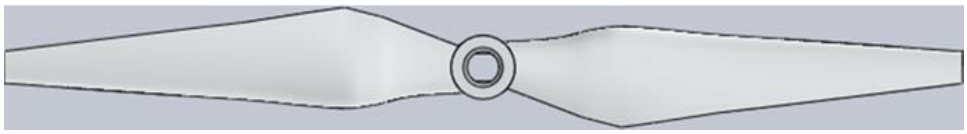

Figure 3. Baseline propeller

Saw-tooth serration, as a feature, always added to the trailing edge of the propeller in the 2D flat plate and airfoil studies. Meanwhile, in the rotating motion study performed by Oerlemanse, the author directly added the serration on the trailing edge of the wind turbine at the tip region[15]. Therefore, in present study, three different sizes of saw-tooth serration were added to the trailing edge of the baseline propeller, which are shown in figure 4. The uniform serrations

have width/height ratios (λ/h) of 0.6, 0.9, and 1.2, and have a 6mm height (2h). As mentioned before, in order to reduce the trailing edge noise, the height of the serration should be larger than a quarter of boundary layer thickness at the trailing edge, and the inclined angle cannot be larger than 45 degrees. The present study's choice of a 6mm height will satisfy this condition. In addition, all of the width/height ratios used in this study are lower than 4.

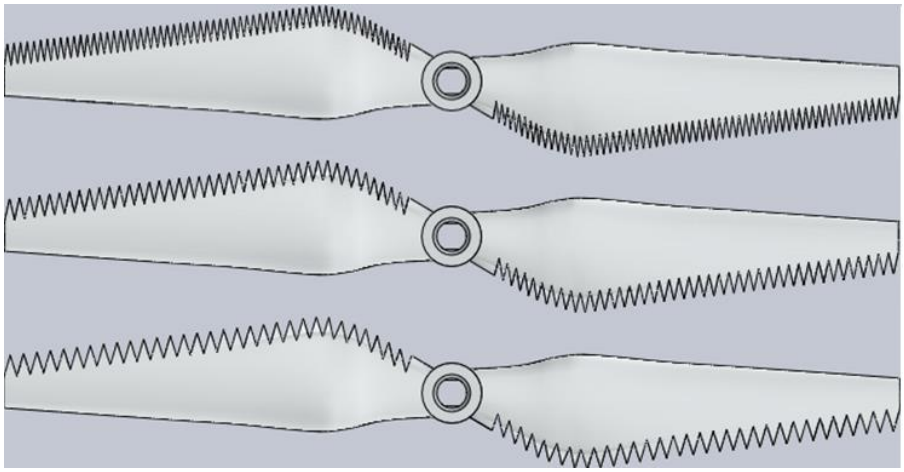

Figure 4. Saw tooth serrated trailing edge propellers

2.2 Experimental setup for the measurements

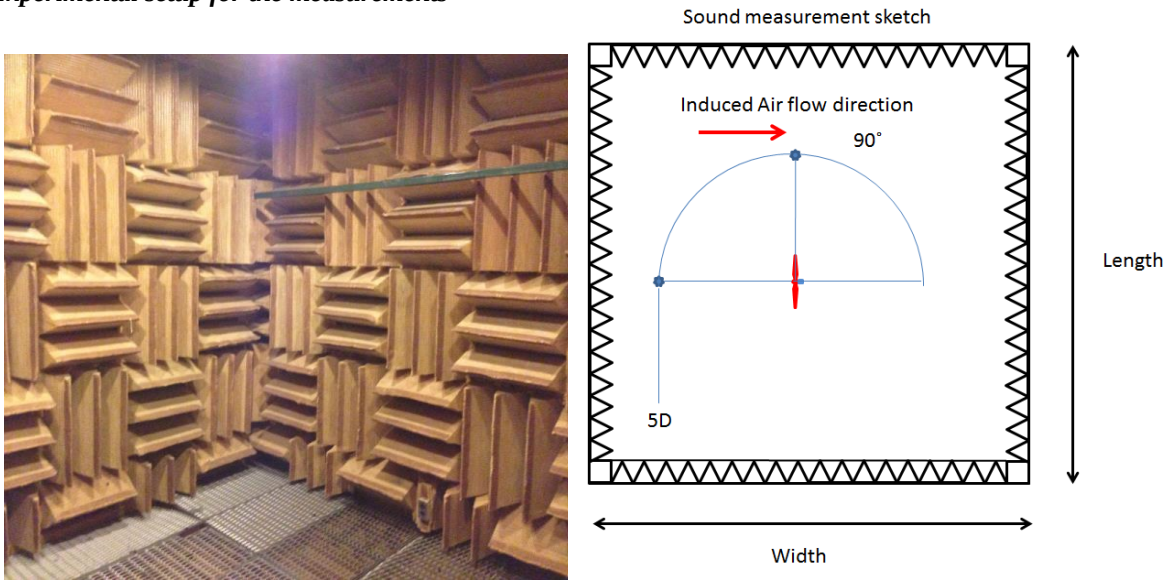

(a) (b)

Figure 5. The anechoic chamber used for aeroacoustic measurements and the sound measurement sketch

The sound at the hover flight condition was measured in an anechoic chamber (as shown in Figure 5 (a)) located in the Department of Aerospace Engineering at Iowa State University. The chamber has dimensions of 12*12*9 feet with a 100Hz cut-off frequency. Figure 5 (b) shows the sketch of the sound measurements. The red arrow represents the induced airflow direction, and the blue points represent the test location. The spectrum measurement was conducted at 0 degrees and 5D away from the propellers. The distance of 5D was chosen because it represents the distance that is considered as far field. In the near field, turbulence levels are high, which would affect the sound measurement.

In addition to the sound measurement, the aerodynamic forces and flow field measurements were also conducted at hover and forward flight conditions. Figure 6 shows the schematic of the experimental setup used in the present study for the hover motion. A 0.2 diameter clearance gap was maintained between the propeller and the support tower. The power used to drive the motor to rotate was provided by a direct current power supply. The UAV propeller was

connected to a function generator via an electronic speed controller. The rotational speed of the propeller was controlled by adjusting the duty cycle of the output signal from the function generator. During the experiment test, the rotational speed of the propeller was measured by tachometer. A high-sensitivity force-moment sensor (JR3 load cell) was used to measure the force and moment, and the precision of this sensor for force measurements was ±0.1N (± 0.25% of the full range). A high-resolution digital PIV system was used to measure the flow field in order to quantify the detailed flow structures around the propeller. An interrogation window with 32×32 pixels and a 50% effective overlap was used to calculate the instantaneous velocity vectors. In order to determine the ensemble-average wake flow statistics and detailed flow structure at certain phase angles both "free-run" and "phase-locked" PIV measurements were conducted in this study. The ensemble-average results were obtained from 1000 frames of instantaneous PIV measurements. For the phase-locked PIV measurements, the phase-averaged flow velocity at certain phase angles ranged from 0 to 150 degrees, with 30 degree increments calculated from 255 frames of the instantaneous PIV measurements. The air was seeded with ~1μm water based droplets by using fog generation. The illumination was provided by an Nd:YAG laser generator with a power of 200mJ per pulse at a wavelength of 532nm. The laser sheet thickness was set to around 1mm at test section. A high-resolution (2048x2048 pixels) charge-coupled device (CCD) camera with an axis perpendicular to the laser sheet was used to capture the raw images. The camera and Laser generator were connected to the computer via a Digital Delay Generator, which controlled the timing of the images captured and the laser illumination. A second digital delay generator was used to modify the signal, in order to achieve the "phase locked" PIV measurements. In the forward flight condition, the pitch angle varies. The test conditions can be found in table 1.

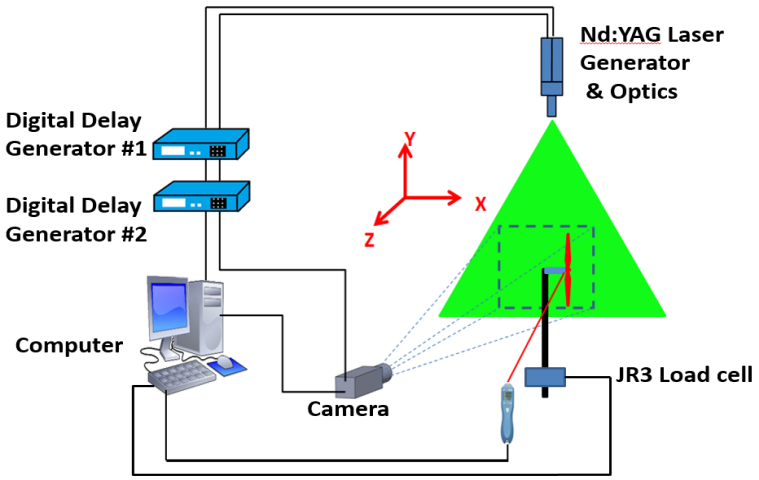

Figure 6. Experimental setup for force and PIV measurements at hover flight motion

Table1. Test conditions at hover flight motion

Blade type	Rotational direction	Voltage Condition	Rotational speed (RPM)
Baseline propeller	CCW (Counter Clock-wise)	11.1	0-6000
Propeller with Saw-tooth serration at λ/h=0.6	CCW (Counter Clock-wise)	11.1	0-6000
Propeller with Saw-tooth serration at λ/h=0.9	CCW (Counter Clock-wise)	11.1	0-6000
Propeller with Saw-tooth serration at λ/h=1.2	CCW (Counter Clock-wise)	11.1	0-6000

Figure 7 shows the experimental setup of the forces and flow field measurements at the forward flight condition. Different from hover motion study, the measurements were conducted inside of a low turbulent wind tunnel located in the aerospace engineering department at Iowa State University. A 10m/s wind speed was used to represent the forward flight speed, which is a typical flying speed of small UAVs in forward flight. In reality, due to the wind drag

acting on a floating aircraft, the rotor would have a pitch angle to maintain the lift and compensate the wind drag. For a given small UAV, the pitch angle is fixed at given wind speed. However, for a fundamental isolated propeller study, 4 pitch angles (-3°, -5°, -10°, and -15°) were used in current study to represent different body configurations. All of the equipment used in forward flight were same as the one used in hover motion. The test conditions are listed in table 2.

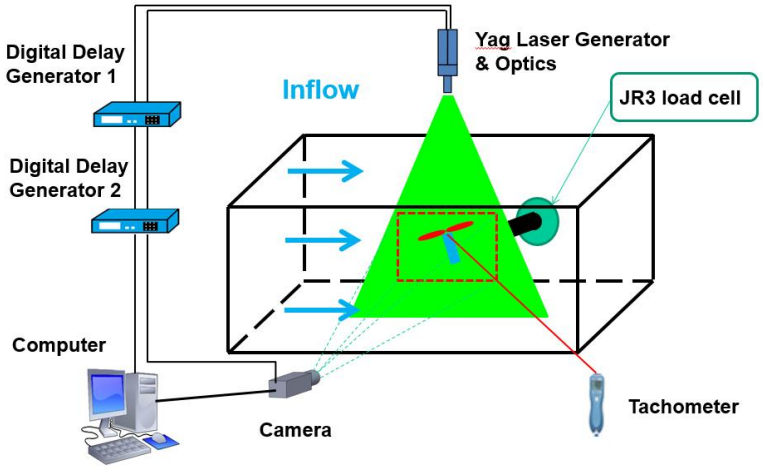

Figure 7. Experimental setup for force and PIV measurements at forward flight motion

Table 2. Test conditions at forward flight motion

Propeller type	Rotational direction	Voltage Condition	Rotational speed (RPM)	Pitch angle
Baseline propeller	CCW	11.1	0-6000	-3°, -5°, -10°, -15°
Propeller with Saw-tooth serration at λ/h=0.6	CCW	11.1	0-6000	-3°, -5°, -10°, -15°
Propeller with Saw-tooth serration at λ/h=0.9	CCW	11.1	0-6000	-3°, -5°, -10°, -15°
Propeller with Saw-tooth serration at λ/h=1.2	CCW	11.1	0-6000	-3°, -5°, -10°, -15°

III. Measurement results and Discussions at hover flight motion

3.1 Aerodynamics force measurement results at hover motion

The aerodynamic force measurements were conducted on the baseline propeller, as well as 3 different serration sized propellers at different rotational speeds. As shown in figure 8, the design thrust is denoted by a dashed line and the results of the different propellers are represented by different colors. The symbols represent the measurement results. Each symbol indicates an average value of 30 seconds of force measurements with a 1000Hz sampling frequency. The saw tooth serrated trailing edge (SSTE) propellers with λ/h ratios of 0.6, 0.9, and 1.2 required the same power input to generate equal thrust compared to baseline propeller. It is illustrated that the three SSTE propellers with λ/h ratio of 0.6, 0.9, and 1.2 have almost same aerodynamics performance compared to baseline propeller. Meanwhile, the rotational speed of these three SSTE propellers are slightly lower than the baseline propeller. As mentioned before, the serration at trailing edge will increase the drag coefficient. Under constant power input, the increasing drag would cause the rotational speed decreasing.

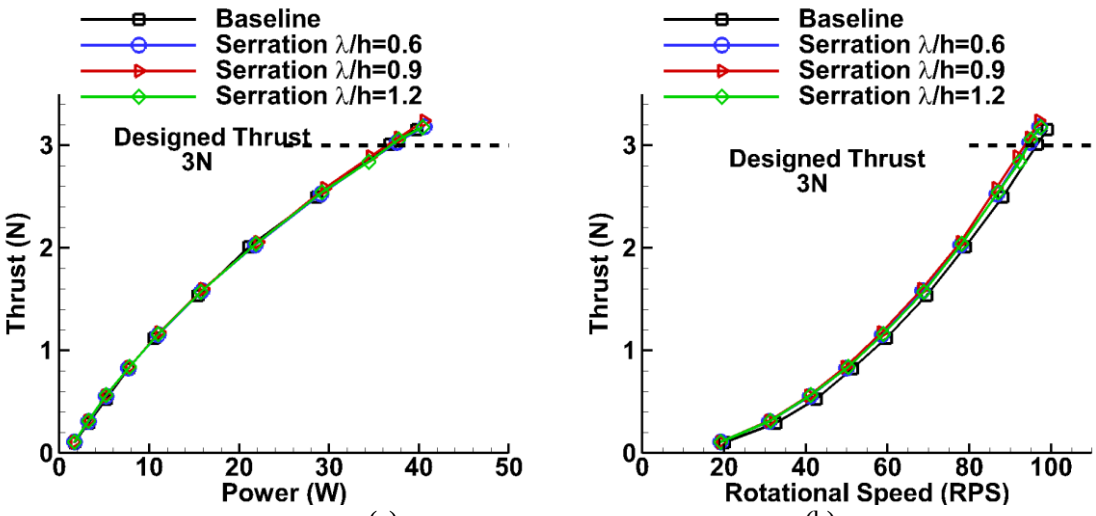

Figure 8. force measurement results of 4 propellers at different rotational speeds

3.2 Sound measurement results at hover motion

The sound measurements were conducted to the 4 propellers at hover motion, which is a unique flight condition for vertical take-off and landing aircraft, where the thrust generated from the propeller equals to the aircraft weight. In the current study, the propeller generated 3 N thrust at hover motion. As mentioned before, the SSTE propellers with λ/h ratio of 0.6, 0.9, and 1.2 had almost same rotational speed with the baseline propeller. According to Lighthill's acoustic analogy, the sound propagated from a propeller is proportional to its velocity. The figures on the left illustrate the sound pressure levels (SPL) at low frequencies. The SPL at high frequencies are shown on the right. The SPL was calculated by equation 1, where reference pressure, p_{ref} was 2μPa. The peaks shown in figure 9 (a) are called tonal noise components, which are associated with blade passing frequency (BPF). The BPF is defined as rotational speed multiplied by the number of blades. Due to the rotational speed difference, the peak shift can be viewed clearly. Compared with baseline propeller, the SPL of the SSTE propellers for all three serration sizes at low frequencies was almost the same. However, the noise attenuation due to the serrated trailing edge is apparent at higher frequencies. This is because the serrated trailing edge reduced the turbulent-boundary layer trailing edge noise as well as trailing edge bluntness vortex shedding noise. The serration at trailing edge would increase the mixing of the turbulent flow and reducing the correlation length of the turbulent. There the scattering efficiency of the turbulent boundary layer trailing edge noise will be decreasing. The detailed flow structure provided in the flow field measurements will clearly show the wake deformation. The trailing edge bluntness vortex shedding noise can be neglected when the thickness of the trailing edge is smaller than the 30% of the boundary layer displacement thickness[17]. In current study, the thickness (t) at trailing edge is 0.29mm. The smallest boundary-layer displacement thickness (δ^*) is $0.04mm$, which was calculated by equation 2[18], where the C is the chord length. The chord Reynold number is 53,000, and the smallest chord length is 8mm. The bluntness parameter (t/δ^*) is larger than 0.3. Therefore, the trailing edge bluntness vortex shedding noise displayed in the spectra are expected. By integrating the SPL at all frequencies of the 4 propellers, it was found that the SSTE propellers with λ/h ratios of 0.6, 0.9, and 1.2 reduced the noise 0.9dB, 1.4dB, and 1.6dB, respectively. This means that a wide serration size benefits noise reduction more. This trend has also been reported by Moreau[13] and Chong[19].

$$SPL\ (dB) = 20\ log_{10}\left(\frac{p}{p_{ref}}\right)(dB) \quad (1)$$

$$\delta^* = \frac{0.37C}{8Re_C^{0.2}} \quad (2)$$

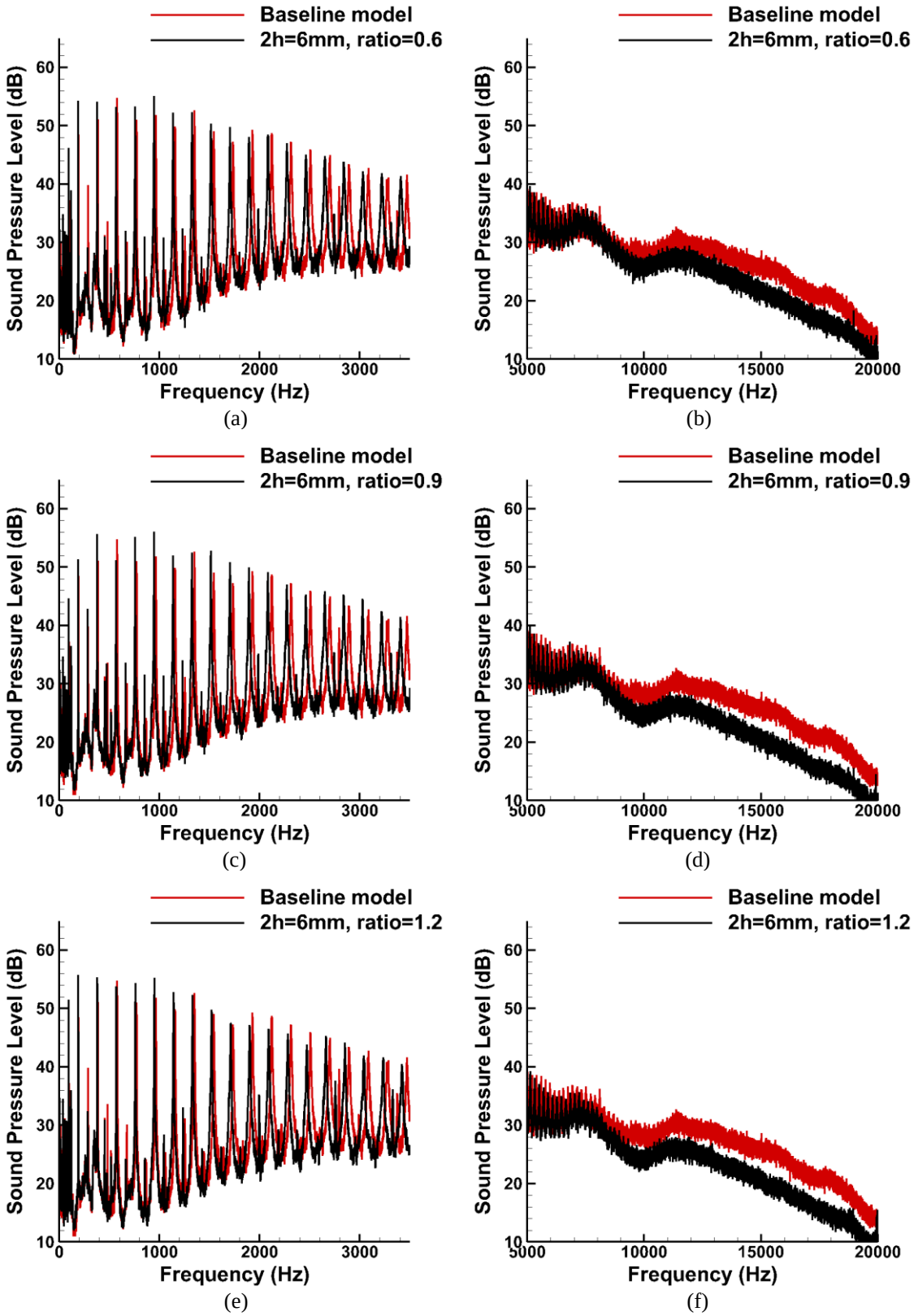

Figure 9. Sound spectra distributions comparison between the baseline propeller and SSTE propellers

3.3 Flow field measurement results at hover motion

As mentioned previously, the flow filed measurements of the 4 propellers were achieved by a high-resolution PIV system. Like the sound measurements, the flow structure measurements were also conducted at the hover motion. Figure 10 shows the "free run" PIV measurement results of the baseline propeller. The term "free run" means the image taken was not harmonic with the propeller rotation. In the plot, the X and Y axes were normalized based on the propeller radius (120mm). The red arrow on the top-left corner indicates the induced airflow direction. Figure 10 (a) is the raw image taken by the camera. Four tip vortex structures were revealed downstream of the propeller in a queue, which can be viewed clearly from the instantaneous and "phase locked" PIV measurement results. In addition to the tip vortex, the vortex structure due to the blunt body effect of the motor and the vorticy fluctuations can be seen clearly in figure 10 (b). In terms of mean velocity, the ensemble-averaged PIV measurement results are shown in figure 10 (c). Three typical flow regions can be easily identified here. The large blue region is the quiescent flow region, where the flow velocity is small. The region above the propeller is the inflow region. With the force generated by the propeller rotation, the flow was sucked into the rotating plane and pushed downward to generate thrust. The colorful region below propeller is the induced flow region. The flow velocity here is higher compared with other two regions. Due to the low pressure at the high velocity region, the flow shinks inward. Figure 10 (d) shows the ensemble-averaged vorticity results. Instead of clear tip vortex structures, the tip vorticy region and the vortices after the motor are very obvious; both of them dissapated very rapidly. Due to this dissipation, the increasing tip vortices region can be clearly seen.

In order to better understand the flow phenomena and aerodynamic effect due to the saw-tooth serrated trailing edge, "phase-locked" PIV measurements were conducted to obtain the detailed flow characteristics in the downstream. In present work, the flow characteristics were studied at six different phase angles range from 0 to 150 degrees with an increment of 30 degrees. The velocity and vorticity distributions of the "phase-locked" PIV measurement results of the baseline propeller at 0° and 60° phase angles are shown in figure 11. The 0 degree phase angle means the propeller is just crossing the measurement plane. Just like the "free run" PIV measurement results, three typical flow regions could be clearly obseved. One phenomenon which was not captured by the "free run" PIV measurement is the periodic velocity drop close to the boundary between the induced flow region and quiescent region in the near wake (within one radius). This is mainly due to the blade tip cutting the flow, and results in the formation of the tip vortices. Tip vortex structures, a typical feature of the weak flow, are generated at the tip of a blade because of the pressure difference between pressure side and suction side of an airfoil. This structure can be viewed clearly in figure 11 (c) and (d), the vorticity distribution of the "phase-locked" PIV measurement results. As the phase angle increased from 0 to 60 degrees, the tip vortex structure traveled downstream and shrank inwards because the induced velocity was low at the tip and high in the middle, which resulted in a low pressure region in the middle section. At around 0.6 radius downstream, the coming tip vortex structure started to interact with the previous one. At about 1.2 radii downstream, two tip vortices mixed and dissipated. This mixing and dissipation resulted in the tip vortices getting larger while losing their strength, and the core structures disappearing. The vortices due to the blunt body effect of the motor are also observed in the "Phase locked" PIV measurements, which dissipated very fast. Besides tip vortices and the vortices due to the motor, both positive and negative vorticity regions induced by the flow passing propeller trailing edge can be identified from all the plots. Because the velocity gradient was small from tip toward rotating axis, this pair of vortices were almost parallel to the rotating plane. At about one rotor radius downstream, they started to mix with the surrounding wake and dissipated. The strength of this pair of vortices are smaller compared to the tip vortices.

The ensemble-averaged velocity comparison results are shown in figure 12. It can be identified that the mean flow field does not have any distinguishable difference among all of the propellers. From momentum theory, we know that the thrust generated from the propeller is proportional to the induced velocity. At the hover motion, all of the 4 propellers generated equal thrust. These similar flow fields indicated that the serrations did not significantly affect the mean flow. However, the serration would affect the instantaneous flow struture, especilly the flow passing trailing edge. The vorticity distribution results of the 4 propellers at the 90° phase angle are used for comparison. As shown in figure 13, compared with the baseline propeller, the structure and strength of the tip vortices of the three serrated trailing edge propellers were almost the same. The significant flow structure difference is the vortices due to flow passing trailing edge. It was found that the tilting direction of these vorticity pairs of the baseline propeller are different from the SSTE propellers with λ/h ratios of 0.6, 0.9, and 1.2 in the downstream between 0.5R to 1.5R. This is due to the velocity difference in the downstream, which is the result of the serrated trailing edge. León[20] illustrated that the flow passing the serration will generate a pair of vortices. Due to the pressure difference between the two serrations, the vortex pairs will generate upwash flow between the serrations, and downwash flow at the tip of serration. This vortex pair may benefit the mixing process and change the pressure distribution after the trailing edge, resulting in a

velocity change after the flow passing trailing edge. The velocity distributions of the 4 propellers at the different downstream locations in the wake are given in figure 14. At 0.2R downstream, all of the three SSTE propellers generated higher velocity at the tip and lower velocity at the middle span compared to the baseline propeller. At 0.7R downstream, instead of one hump of the baseline propeller, the velocity distributions of the SSTE propellers with λ/h ratios of 0.6, 0.9 and 1.2 had double humps. Further downstream, the velocity distributions of the 4 propellers were the parabolic shape with peak value shifts. These velocity distribution differences indicated that the serration at trailing had the effect on the flow passing it. One interesting phenomenon is the velocity distributions of the SSTE propellers with λ/h ratios of 0.9 and 1.2 are almost same. Refer to the sound measurement results, these two propellers had better noise reduction effect.

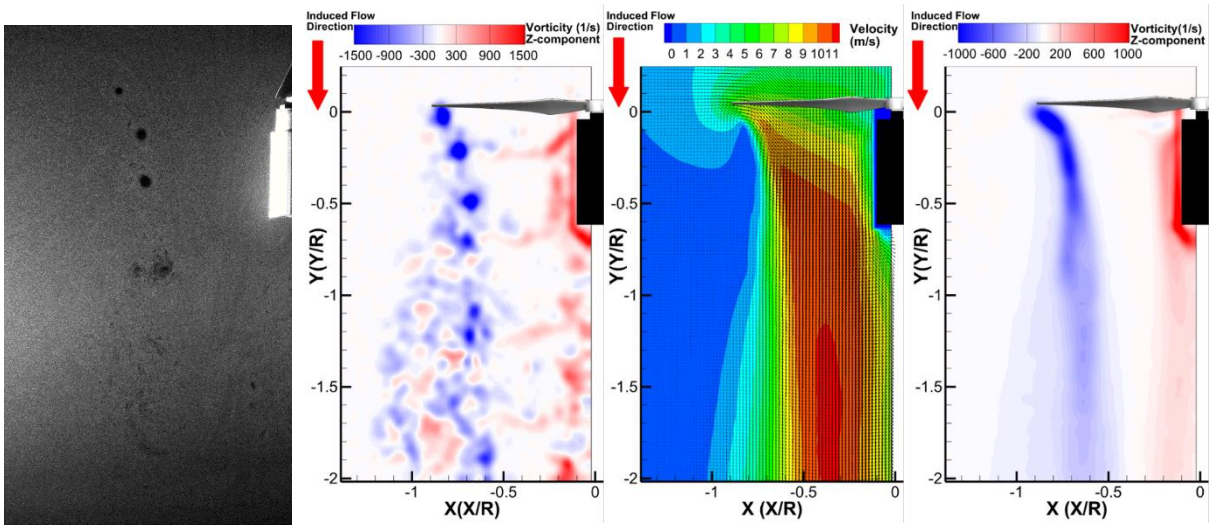

(a) Raw image (b) Instantaneous vorticity (c) averaged velocity (d) averaged vorticity

Figure 10. "Free run" PIV measurement results of baseline propeller at hover motion

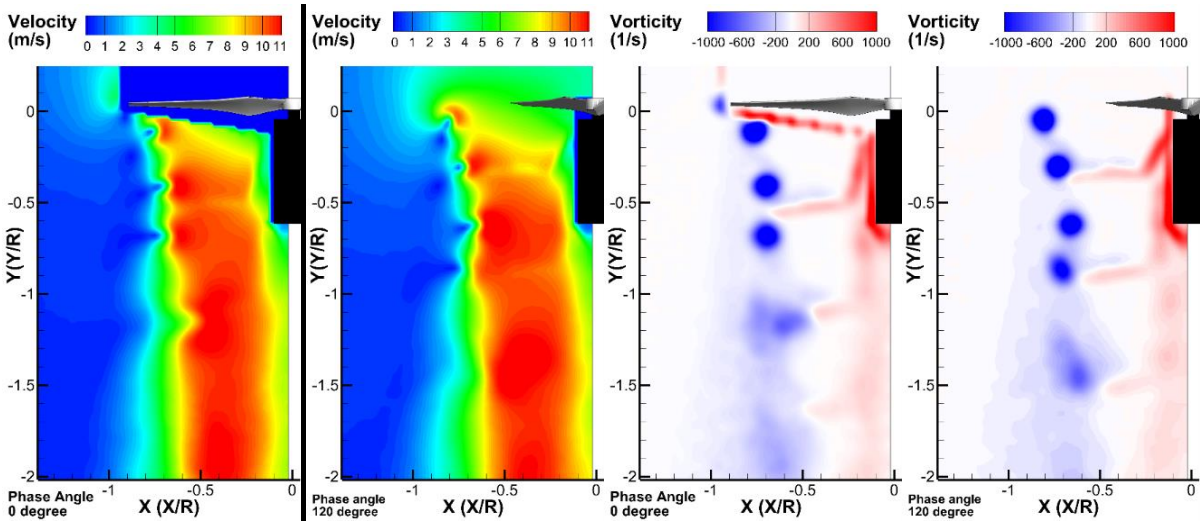

(a) (b) (c) (d)

Figure 11. "phase-locked" PIV measurement results at hover motion

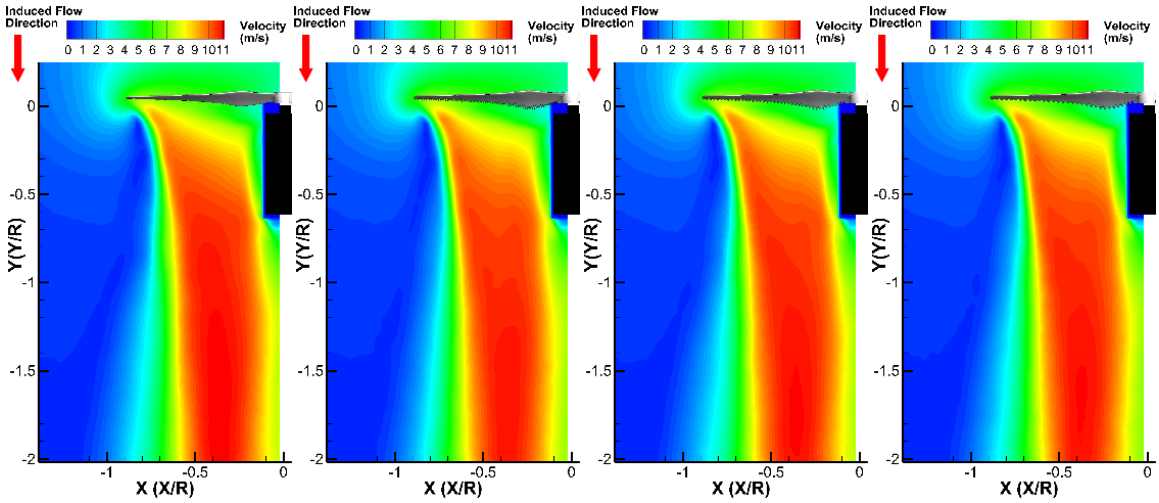

(a) baseline (b) serration λ/h=0.6 (c) serration λ/h=0.9 (d) serration λ/h=1.2

Figure 12. Ensemble average velocity comparison at hover motion

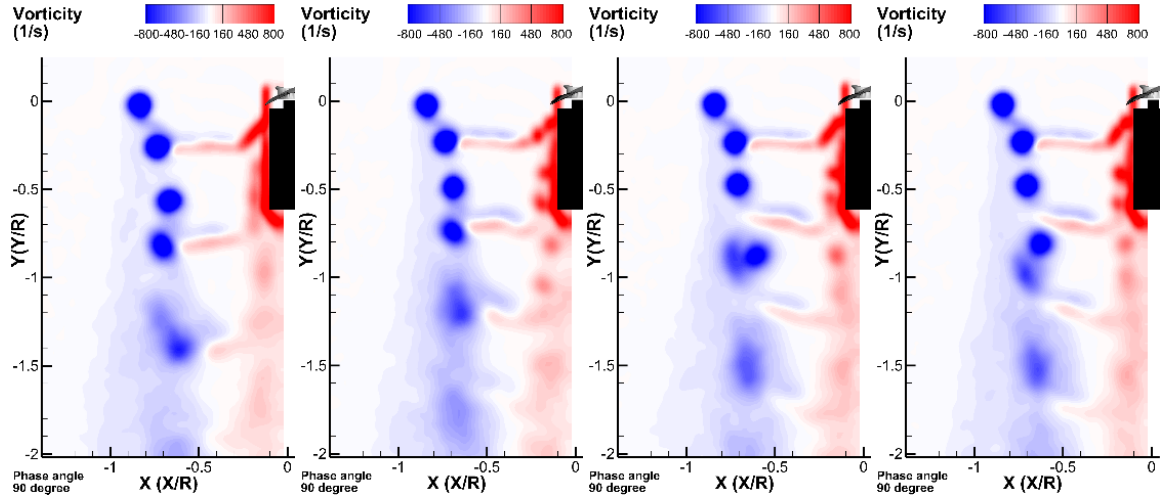

(a) baseline (b) serration λ/h=0.6 (c) serration λ/h=0.9 (d) serration λ/h=1.2

Figure 13. Vorticity comparison at 90 degree phase angle at hover motion

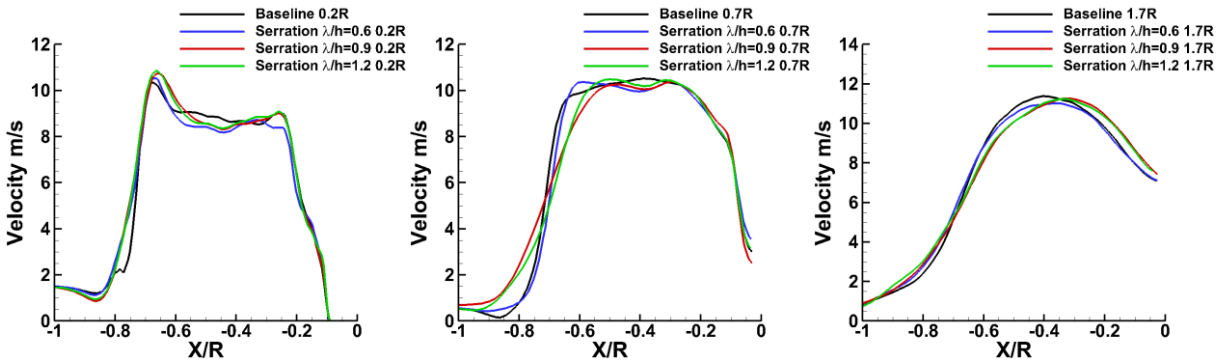

(a) 0.2R downstream (b) 0.7R downstream (b) 1.7R downstream

Figure 14. Velocity comparison are different downstream location

IV. Measurement results and Discussions at forward flight motion

4.1 Aerodynamics force measurement results at forward flight

In addition to the hover motion analysis, the aerodynamic force was also measured in the forward flight condition. Since the smallest serration size propeller had poor aerodynamic performance due to geometry deforming, the forward flight study was only focused on the baseline propeller and the SSTE propellers with λ/h ratios of 0.6, 0.9, and 1.2. The power versus lift results at different pitch down angles are shown in figure 15. Compared to the baseline propeller, all three of the serration propellers required the same power to generate equal thrust. With the pitch down angle increasing, more power was required to create same lift. Figure 16 shows the lift versus rotational speed comparison results of the 4 different propellers. Unlike in the hover motion test, all three SSTE propellers rotated slower than the baseline propeller at forward flight when they generated the same lift. In forward flight, the baseline propeller rotated about 5 Hz faster than the SSTE propellers. The three SSTE propellers had same rotational speed and required same power input to produce equal lift, which indicated that the serration size did not affect the lift generation. As mentioned by Gruber, the serration has no significant effect on the lift generation[11]. However, it would slightly increase the drag coefficient. Under constant torque, this drag increase would cause the rotational speed to decrease. With this change in the rotational speed, the operating angle of attack would also vary. This phenomenon would lead to the same lift generation. In order to generate same lift, the rotational speed of all of the propellers would need to increase to match the effects of the pitch down angle increasing.

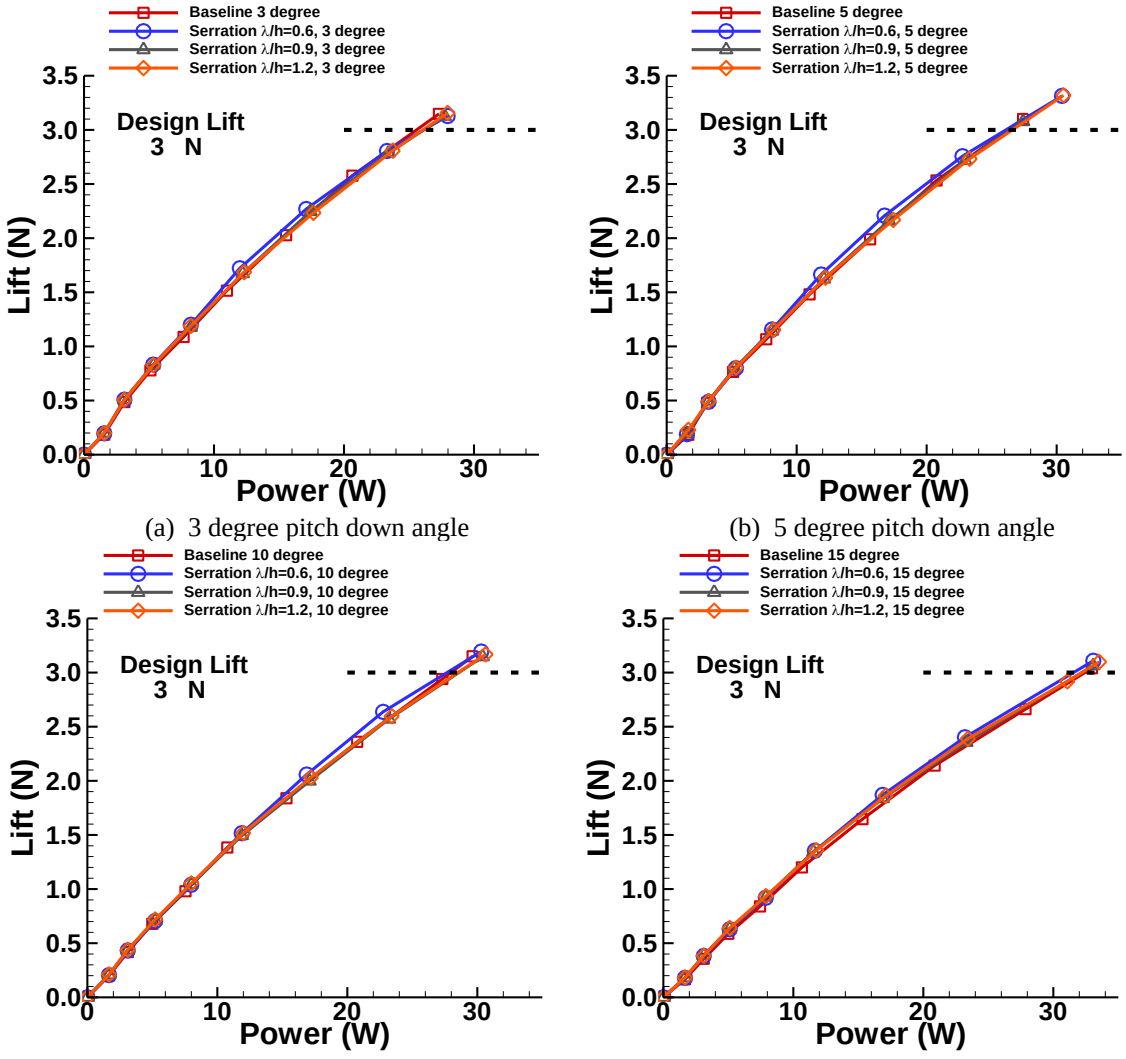

(a) 3 degree pitch down angle

(b) 5 degree pitch down angle

(c) 10 degree pitch down angle

(d) 15 degree pitch down angle

Figure 15. Lift vs power at different pitch angle of baseline and serrated trailing edge propellers

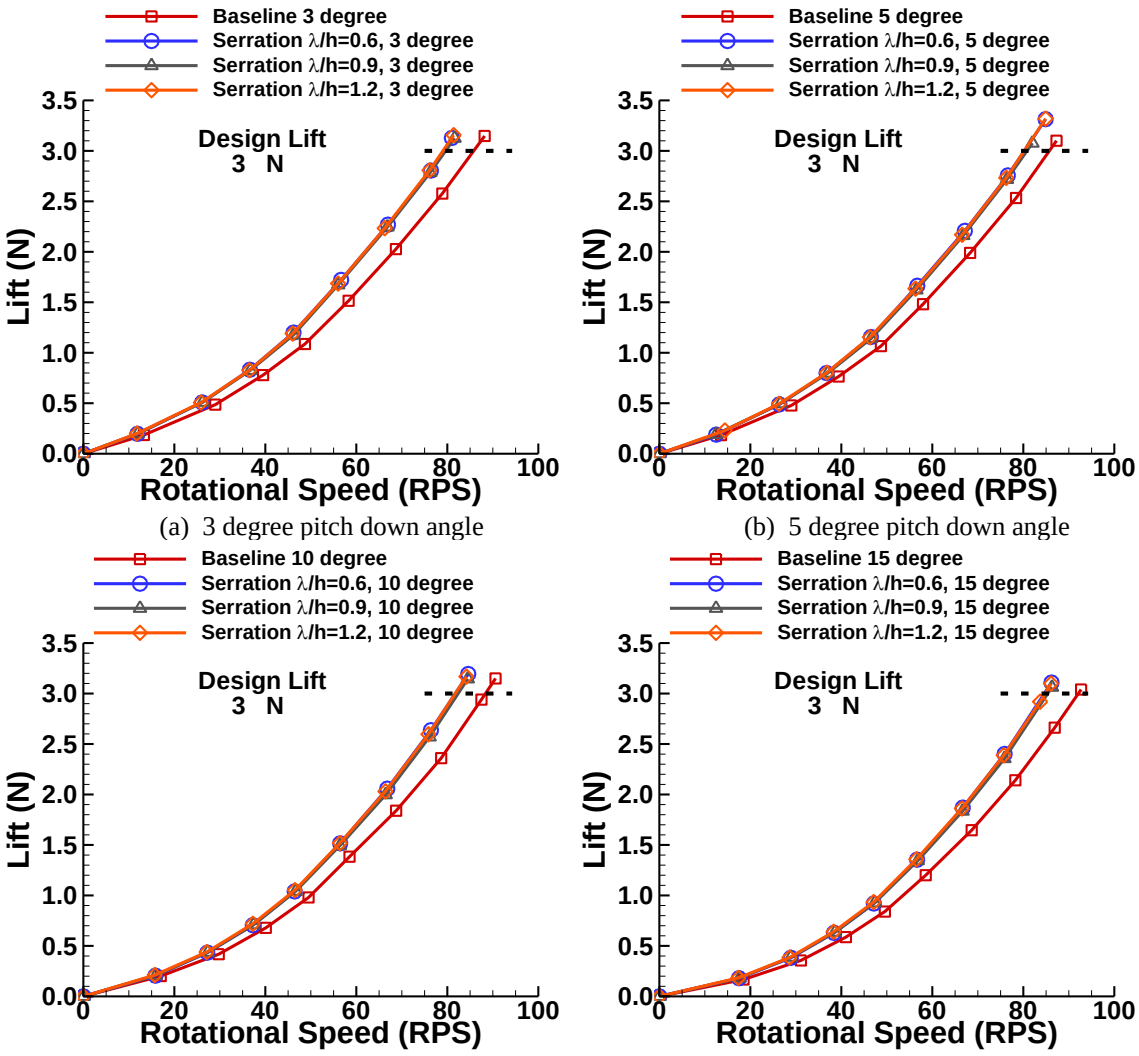

(a) 3 degree pitch down angle

(b) 5 degree pitch down angle

(c) 10 degree pitch down angle

(d) 15 degree pitch down angle

Figure 16. Lift vs rotational speed at different pitch angle of baseline and serrated trailing edge propellers

4.2 Flow field measurement results at forward flight

The flow field measurements were also conducted in forward flight. Since the propeller is not perpendicular to the incoming flow, the relative velocity of the two side blades will be different. As shown in figure 17, the blade which rotates into the incoming flow is the advacing blade, where relative velocity is the rotational speed plus the incoming flow speed at 0 degrees pitch down angle. The blade which rotates with the incoming flow called retreating blade, where relative velocity is the rotational speed minus the incoming flow speed at 0 degrees pitch down angle. Therefore, at certain region close to the center, the incoming flow velocity is higher than the rotaitonal speed. As a result, the air flows from trailing edge to the leading edge. This region is called reverse flow region. The velocity distribution sketch of longitudinal and lateral inflow are also provided in this figure. Figure 18 shows the "free run" PIV measurement results of the 4 propellers with 10m/s wind speed and 10 degree pitch down angle in the middle plane. The two high velocity regions in the wake can be clearly viewed in all the plots. This is induced by the propeller rotation. The vorticity due to the flow passing motor also can be viewed down to the rotor. The flow field of the SSTE propellers were very similar to the baseline propeller. By tracking the velocity distributions at different downstream locations (1.0R and 1.5R), a slight velocity change due to the serration could be found in figure 19. At 1.0R downstream, the three serrated trailing edge propellers had almost same profile. This indicated that the serration sizes did not affect the mean flow. The baseline propeller generated higher induced velocity from 0.4R to 0.8R compared to the serrated trailing propellers.

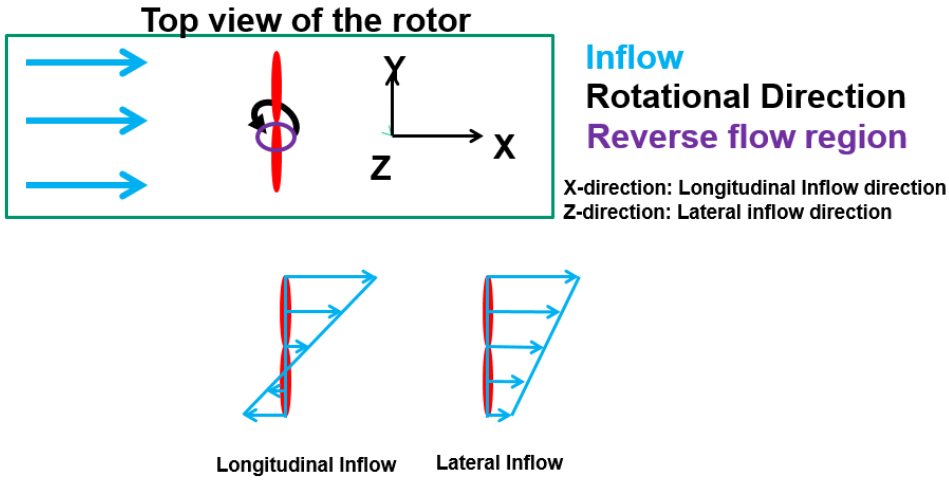

Figure 17. flow sketch at forward flight

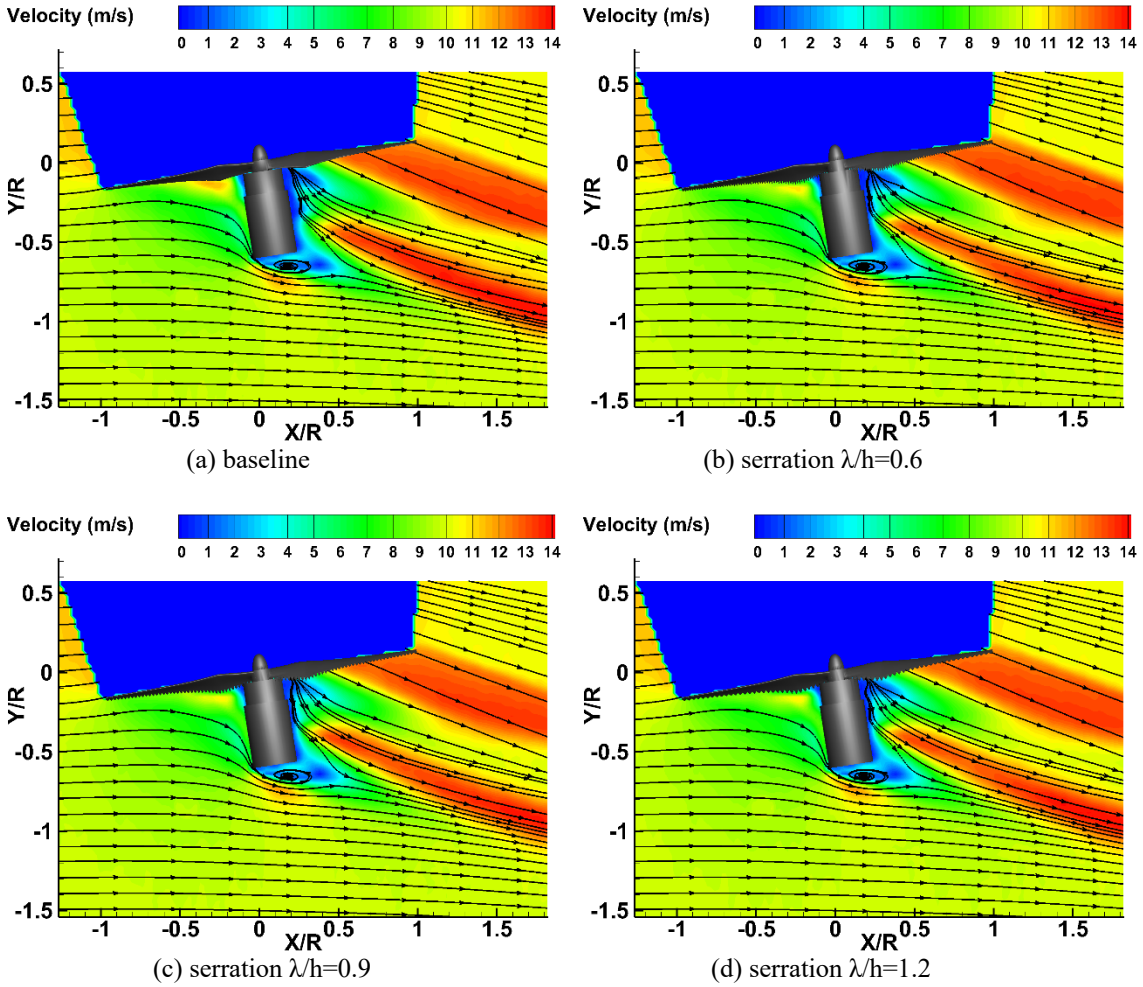

(a) baseline (b) serration λ/h=0.6

(c) serration λ/h=0.9 (d) serration λ/h=1.2

Figure 18. Ensemble-averaged velocity of the "free-run" PIV measurement results at forward flight

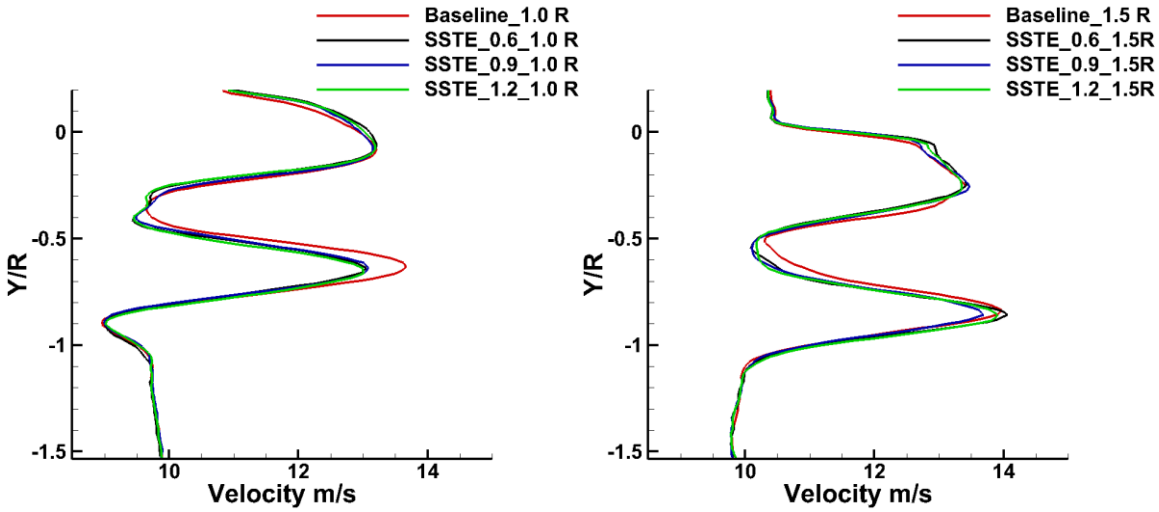

Figure 19. Velocity comparison are different downstream location in forward flight

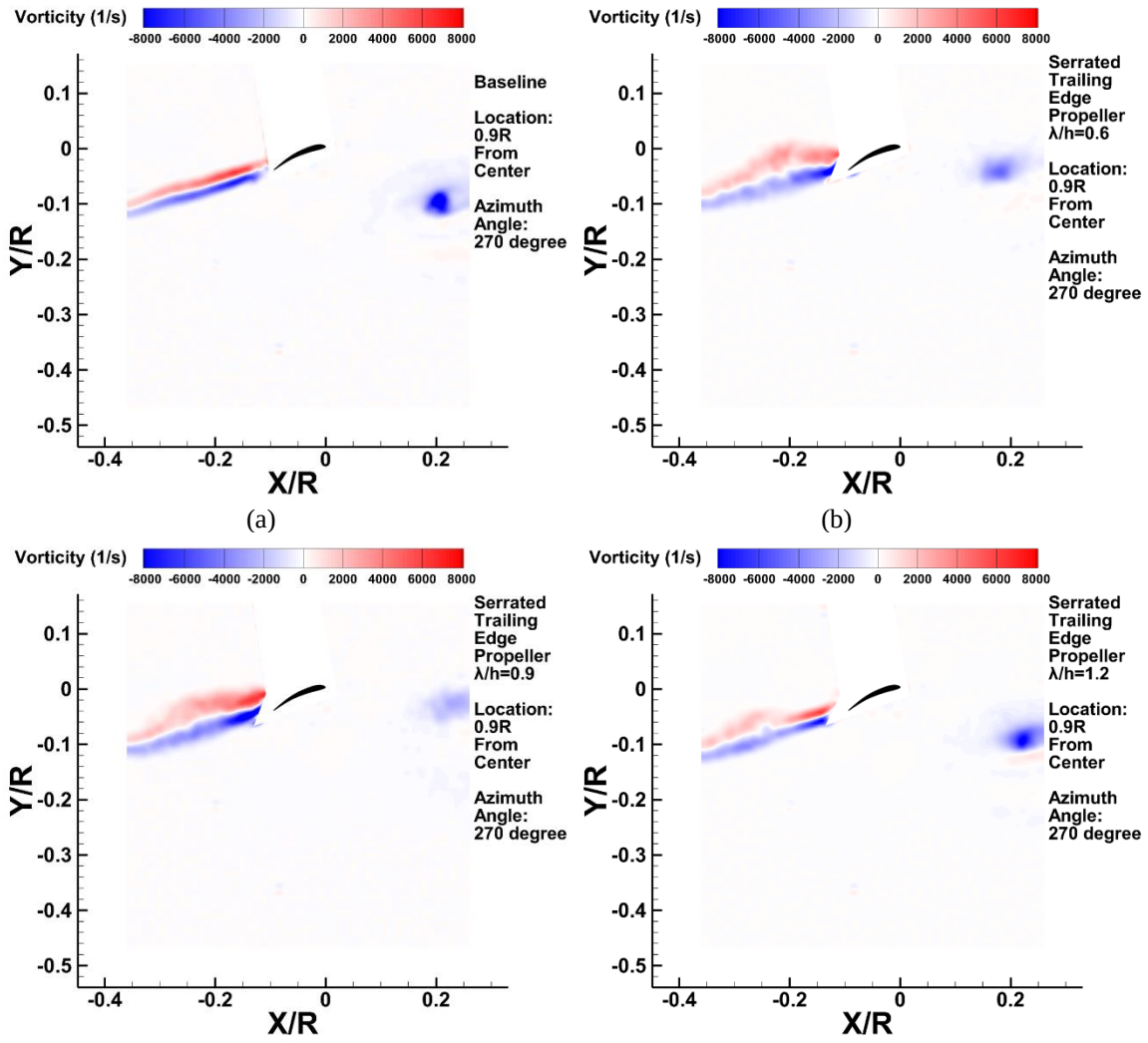

Figure 20. "Phase locked" PIV measurement results at ψ=270° at 90% radius

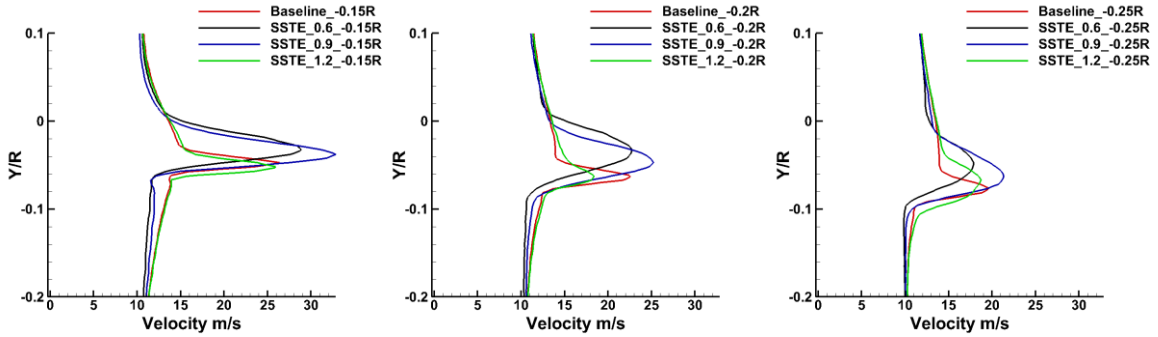

Figure 21. Velocity comparison are different downstream locations

Chord section "phase locked" PIV measurements were also conducted at 270° azimuth angle and at 90% radius from the rotating center. The vorticity distribution results of the 4 propellers at 0.9R are shown in figure 20. The blue region at 0.2R in the front of the airfoil is the tip vortex generated from another blade. The tip vorticy dissapation speed of the SSTE propellers is faster compared to the baseline propeller. The vorticies due to the flow passing trailing can be clearly viewed downstream of the airfoil. Due to the serration, the wake region increases significantly, which has been obseved by Finez[21], Gruber[12], and Moreau[13] in their 2D airfoil measurements. One interesting phenomenon is the wake geometry of the serrated trailing edge propeller with λ/h of 1.2. It started with a similar wake size as the baseline propeller. A short time later, the wake size increased significantly. The other two serrated trailing edge propellers showed the large wake size start directly from the trailing edge. Figure 21 shows the velocity distribution comparison results of the 4 propellers at the three different downstream locations of the trailing edge. The propellers with serration sizes of λ/h equal to 0.6 and 0.9 had a large wake region compared to baseline propeller. The serrated trailing edge propeller with a λ/h of 1.2 had a similar wake size to the baseline propeller at -0.15R downstream. This phenomenon was also observed by Moreau[13]. In his research, the plate with narrow serration generated a large wake size, and the plate with wide serrations generated a similar wake to reference plate. As the flow traveled to the downstream, the decrease of the wake velocity and the increase of the wake region can be clearly visualized for the SSTE propeller with λ/h of 1.2. Probably, the best serration size is the one that does not increase the wake size significantly, but instead increases the turbulent mixing.

V. Conclusion

An experimental study on the aerodynamic and aeroacoustic performance of a baseline propeller and several saw-tooth serrated trailing edge (SSTE) propellers with different serration sizes (λ/h=0.3, 0.6, 0.9 and 1.2) was conducted at hover and forward flight conditions. The sound measurement results at hover motion revealed that the SSTE propellers could reduce the noise levels. We also found that the large serration had better noise attenuation effects than the smaller serration sizes. The comparison results of the force measurements among baseline model and SSTE propellers revealed that the saw-tooth serrated trailing edge had no significant effect on the aerodynamic performance at low Reynolds numbers (5×10^4) at hover flight. The force measurement results at forward flight indicated that the SSTE propellers could maintain the same lift while reducing the rotational speed. The PIV measurement results revealed that the SSTE propellers with different serration sizes generated almost same mean flow at hover and forward flight conditions. However, it significantly changed the wake shape and size of the flow passing the trailing edge. This phenomenon increases the flow mixing at the tailing edge. For small size propellers, the material strength needed to be considered carefully to account for undesirable structural effects associated with serration sizes that are too fine. Otherwise, the serration deformation would significantly reduce the aerodynamic efficiency and increase the noise level.

Acknowledgments

The research work was supported by National Science Foundation (NSF) under award number of IRES-1064235. The authors want to thank Dr. Kai Zhang, Dr. Wenwu Zhou, and Mr. Brandon Weigel of Iowa State University for their help in conducting the experiments.

References

[1] Floreano, D., and Wood, R., "Science,technology and the future of small autonomous drones," *Nature*, vol. 521(7553), 2015, pp. 460–466.

[2] BI INTELLIGENCE, "The Drones Report: Research, Use Cases, Regulations, and Issues - Business Insider" Available: http://www.businessinsider.com/the-drones-report-research-use-cases-regulations-and-issues-2016-4-28.

[3] MarketsandMarkets, "Small Drones Market worth 10.04 Billion USD by 2020" Available: http://www.marketsandmarkets.com/PressReleases/small-uav.asp.

[4] Hoffmann, G., Huang, H., Waslander, S., and Tomlin, C., "Quadrotor Helicopter Flight Dynamics and Control: Theory and Experiment," *AIAA Guidance, Navigation and Control Conference and Exhibit*, 2007.

[5] Ditmer, M., Vincent, J., Werden, L., Tanner, J., Laske, T., Iaizzo, P., Garshelis, D., and Fieberg, J., "Bears Show a Physiological but Limited Behavioral Response to Unmanned Aerial Vehicles," *Current Biology*, vol. 25, Aug. 2015, pp. 2278–2283.

[6] Leslie, A., Wong, K. C., and Auld, D., "Broadband noise reduction on a mini-UAV Propeller," *29th AIAA Aeroacoustics Conference*, 2008, pp. 5–7.

[7] Sinibaldi, G., and Marino, L., "Experimental analysis on the noise of propellers for small UAV," *Applied Acoustics*, vol. 74, Jan. 2013, pp. 79–88.

[8] Brooks, T. F., Pope, S., and Marcolini, M. A., "Airfoil Self-Noise and Prediction," *NASA Reference Publication 1218*, 1989, pp. 1–142.

[9] Howe, M. S., "A review of the theory of trailing edge noise," *Journal of Sound and Vibration*, vol. 61, Dec. 1978, pp. 437–465.

[10] Howe, M. S., "AERODYNAMIC NOISE OF A SERRATED TRAILING EDGE," *Journal of Fluids and Structures*, vol. 5, 1991, pp. 33–45.

[11] Gruber, M., Joseph, P. F., and Chong, T. P., "Experimental investigation of airfoil self noise and turbulent wake reduction by the use of trailing edge serrations," 2010.

[12] Gruber, M., Joseph, P., and Chong, T., "On the mechanisms of serrated airfoil trailing edge noise reduction," *17th AIAA/CEAS Aeroacoustics Conference (32nd AIAA Aeroacoustics Conference)*, 2011.

[13] Moreau, D. J., and Doolan, C. J., "Noise-Reduction Mechanism of a Flat-Plate Serrated Trailing Edge," *AIAA Journal*, vol. 51, Oct. 2013, pp. 2513–2522.

[14] Herr, M., and Dobrzynski, W., "Experimental Investigations in Low-Noise Trailing-Edge Design," *AIAA JOURNAL*, vol. 43, 2005.

[15] Oerlemans, S., Fisher, M., Maeder, T., and K?gler, K., "Reduction of Wind Turbine Noise Using Optimized Airfoils and Trailing-Edge Serrations," *AIAA Journal*, vol. 47, Jun. 2009, pp. 1470–1481.

[16] Eppler, R., *Airfoil design and data*, Springer Berlin Heidelberg, 1990.

[17] Blake, W. K., *Mechanics of Flow-Induced Sound and Vibration V1, 1st Edition*, ELSEVIER ACADEMIC Press, 2012.

[18] Cebeci, T., and Bradshaw, P., "Momentum transfer in boundary layers," *Washington, D.C., Hemisphere Publishing Corp.; New York, McGraw-Hill Book Co., 1977. 407 p.*, 1977.

[19] Chong, T. P., Joseph, P., Vathylakis, A., and Gruber, M., "On the Noise and Wake flow of an Airfoil with Broken and Serrated Trailing Edges," *17th AIAA/CEAS Aeroacoustics Conference (32nd AIAA Aeroacoustics Conference)*, 2011.

[20] Arce Leon, C., Ragni, D., Probsting, S., Scarano, F., and Madsen, J., "Flow topology and acoustic emissions of trailing edge serrations at incidence," *Experiments in Fluids*, vol. 57, May 2016, p. 91.

[21] Finez, A., Jacob, M., Roger, M., and Jondeau, E., "Broadband Noise Reduction Of Linear Cascades With Trailing Edge Serrations," *17th AIAA/CEAS Aeroacoustics Conference (32nd AIAA Aeroacoustics Conference)*, 2011.